Generation of Power-Exponent-Phase Vortex Beam Arrays Based on All-Dielectric Metasurfaces

Jiale Guo, Chuan Shen, Jinkun Hu, Yong Zhou, Cheng Zhang, and Sui Wei

***Abstract*—Optical vortices (OV) with an open shape have a unique function in directional particle transport and collection. A power-exponent-phase vortex (PEPV) has received particular attention as a type of unconventional vortex beam with a large opening and carrying orbital angular momentum (OAM). So far, only the generation methods and properties of an individual PEPV beam have been studied and analyzed. In this paper, we use dielectric metasurfaces instead of the conventional bulky optical device to generate PEPV arrays with a uniform diffracted intensity distribution and a controllable correlation between the topological charge number and the diffraction order. This approach is based on the theory of PEPV and combined with the principle of Dammann grating. The proposed method provides a new platform for various applications of light-matter interactions such as optical communication, optical encryption, and multi-particle manipulation.**

***Index Terms*—Vortex beam arrays, dielectric metasurfaces, Dammann grating, multi-particle manipulation.**

I. Introduction

AN OPTICAL vortex beam is a special type of beam with a helical wavefront with a phase factor $\exp(il\theta)$, where θ is an integer and denotes the topological charge and l is the angular coordinate [1], [2]. In addition, vortex beams are characterized by a circular transverse intensity distribution, phase singularities, and infinite orthogonal orbital angular momentum (OAM) channels. Therefore, vortex beams are widely used in laser optical tweezers [3], [4], [5], optical communications [6], [7], [8], microscopic imaging [9], [10], and other fields.

As a kind of noncanonical optical vortex [11], [12], [13], a power-exponent-phase vortex beam (PEPV) is distinguished from a canonical optical vortex that has a spiral phase that varies uniformly with the azimuth angle, and its phase distribution has a power order relationship with the azimuth angle. In addition, The PEPV beam also carries orbital angular momentum related to the topological charge. Its unique phase distribution makes the transverse intensity distribution of the PEPV a non-closed curve [14], [15]. Compared with fractional-order vortex beams, which are also noncanonical vortices, the PEPV beam has a larger circular intensity opening. Relevant literature suggests that the PEPV beam has unique applications in the field of microscopic particle capture and release [16].

The Dammann grating (DG) is a type of binary optical element (BOE) that can modulate the intensity of light in far-field diffraction orders by adjusting the position of the phase transition point during the cycle [17], [18], [19]. In [20], it gave the transition points required to generate different numbers of diffract orders [20]. The gratings fabricated in this way have a high diffraction efficiency and approach a uniform light intensity distribution in all diffraction orders. As a popular compact planar optical device, the metasurface can modulate the phase, polarization, and amplitude of incident light on the subwavelength scale, replacing bulky optical components such as lenses, spatial light modulators (SLM) [21], [22], and liquid crystal (LC) [23], [24]. Recently, the combination of Dammann grating and metasurface has been used to generate 2D and 3D vortex arrays [25], [26], [27], [28]. However, the application of Dammann gratings to generate noncanonical vortex arrays has not been proposed.

In this paper, we propose a novel approach to convert circularly polarized incident light into an array of PEPV beams in the cross-polarized scattered field using a dielectric geometric metasurface, taking advantage of its highly efficient diffraction efficiency, dispersion-free phase properties, and a phase imprinting method that correlates with the orientations of meta-atoms. The proposed method provides a potential approach for the development of ultra-compact nanophotonic manipulation platforms for various optical applications.

II. Theory

The power-exponent-phase vortex is a noncanonical OV with a phase function expression of the form:

$$\psi = 2\pi l\left(\frac{\theta}{2\pi}\right)^{\alpha} \tag{1}$$

where l denotes the topological charge of the vortex beam, its positive or negative determines the vortex opening direction, θ is the azimuthal angle ranging from 0 to 2π, and α is the power order of the vortex beam. When $\alpha = 1$, in this case, the phase function expression of PEPV is consistent with the canonical OV beam expression. Fig. 1 illustrates the helical phase distributions of a conventional vortex beam and a power-exponent-phase vortex beam. Note that, unlike the "donut-shaped" intensity

Manuscript received 9 January 2024; revised 3 March 2024; accepted 4 March 2024. Date of publication 12 March 2024; date of current version 19 March 2024. This work was supported in part by the National Natural Science Foundation of China under Grant 62271005, in part by the Natural Science Foundation of Anhui Province under Grant 2008085MF209, and in part by the Natural Science Foundation of Higher Education Institutions of Anhui Province under Grant 2022AH050089 and Grant KJ2020ZD02. *(Corresponding author: Chuan Shen.)*

The authors are with the Key Laboratory of Intelligent Computing & Signal Processing, Ministry of Education, Anhui University, Hefei 230601, China (e-mail: libero_jialeG@163.com; shenchuan@ahu.edu.cn; 1436984051@qq.com; 943176956@qq.com; zhangchengahu@163.com; swei@ahu.edu.cn).

Digital Object Identifier 10.1109/JPHOT.2024.3374459

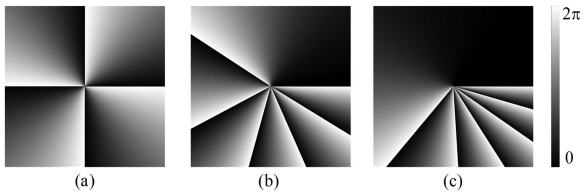

Fig. 1. Spiral phase distributions of the PEPV beam with different power orders α and topological charges l. (a) $\alpha = 1$, $l = 4$; (b) $\alpha = 2$, $l = 4$; (c) $\alpha = 3$, $l = 4$.

distribution of a conventional canonical vortex beam, the phase change rate of the PEPV increases with azimuthal angle due to the presence of the power-order term, resulting in a letter "C" shape of the intensity profile of the beam. In addition, the spot size of helix increases as the topological charge number increases, while the shape of the helix approaches a fixed shape. Increasing the power order results in a more concentrated intensity distribution of the beam.

Consider now the Dammann grating that adjusts the position change of the binary-phase transition point in the cycle. It could present an expected intensity distribution of laser far-field multi-order spectral points, which can effectively solve the problem of uneven energy distribution between different diffraction orders. For the purpose of this discussion, we consider the case of one-dimensional Dammann grating, its transmittance function can be expressed as follows:

$$T_{DG} = \exp\left(i\varphi_{DG}\right) = \sum_{m=-\infty}^{+\infty} C_m \exp\left(i\frac{2m\pi x}{T_x}\right) \tag{2}$$

where C_m is the coefficient of the mth diffraction order and T_x is the period of grating. For a set of desired orders, the values of C_m are equal.

The conventional Dammann vortex grating (DVG) could be obtained by loading the helical phase into the Dammann grating. The transmittance function of a one-dimensional DVG with topological charge can be written as:

$$T_{DVG} = \sum_{m=-\infty}^{+\infty} C_m \exp\left[im\left(\frac{2\pi x}{T_x} + l_0\theta\right)\right]. \tag{3}$$

Suppose that l is nonzero (integer or fractional), the mth diffraction order of the vortex grating carries a topological charge of ml. In this paper, the conventional helical phase is replaced by the power-exponent phase to obtain a power-exponent-phase Dammann vortex grating (PEPDVG), then the resulting expression for its transmittance function becomes:

$$T_{PEPDVG} = \sum_{m=-\infty}^{+\infty} C_m \exp\left\{im\left[\frac{2\pi x}{T_x} + 2\pi l\left(\frac{\theta}{2\pi}\right)^{\alpha}\right]\right\}. \tag{4}$$

Now we would prefer to employ a kind of optical field manipulating element as an interface between the transmittance function and the optical system. Metasurfaces, consisting of a uniform array of nanoscale optical scatterers, can flexibly modulate the amplitude, polarization, and phase of electromagnetic waves on the subwavelength scale. Furthermore, a dielectric geometric phase metasurface combines high efficiency and broadband response. In this paper, as illustrated in Fig. 2, PEPDVGs are straightforwardly realized by utilizing the dielectric geometric metasurface, and the generation of PEPV arrays is achieved in a cross-polarized channel under the incidence of circularly polarized light.

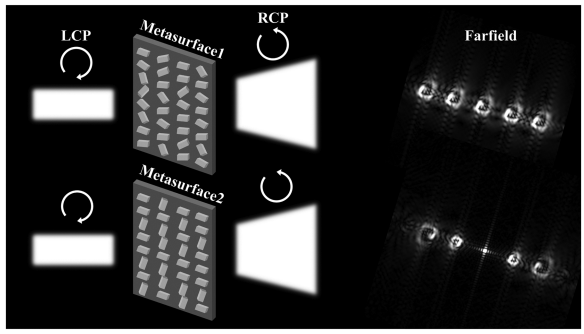

Fig. 2. Schematic illustration of metasurface-based PEPV arrays generation. Incident left circularly polarized light (LCP) illuminates TiO_2 metasurface on glass substrate. Transmitted right circularly polarized light (RCP) contains an array of PEPV beams. Two metasurface types are demonstrated in this work. In the first case, five PEPV beams with the same topological charge are equally spaced generated. In the second case, there is an array of PEPV beams with the different topological charges which are related to the diffraction orders.

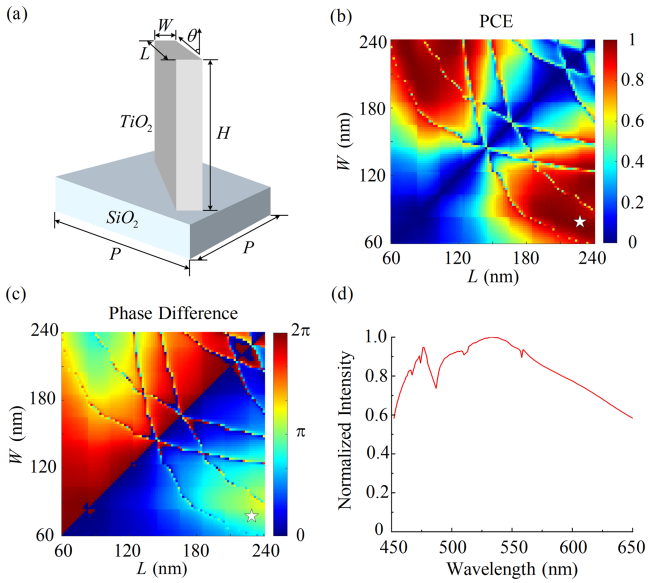

Fig. 3. (a) Structure of each nanopillar unit in one period; (b) Simulated PCE as a function of nanopillars' geometrical parameters L and W at 532 nm; (c) Simulated the phase difference as a function of nanopillars' geometrical parameters L and W under the $x-$ and $y-$ polarized incidence at 532 nm; (d) The normalized cross-polarized component intensity at wavelengths of 450–650 nm.

III. Simulation

A. Design of the Unit of Metasurface

To verify the validity of the proposed method, a number of relevant simulations are performed with FDTD Solutions software (Lumerical Solutions). Firstly, the design of dielectric metasurface will be considered. Fig. 3(a) illustrates a schematic

diagram of the unit cell structure of the proposed metasurface. The unit cell of the metasurface is a rectangular TiO_2 nanopillar with a height of $H = 600$ nm arranged on a silica substrate with a lattice constant of $P = 350$ nm according to a certain in-plane orientation angle. Among them, TiO_2 nanopillars are used as meta-atoms because they have superior performance (e.g. high refractive index and low loss) in the visible wavelength band. Moreover, the orientation angle of the nanopillars with respect to the fast axis has a simple correspondence with the geometrical phase [or Pancharatnam-Berry (PB) phase] generated during the evolution of the cross-polarized state of circularly polarized light. Note that, $\varphi = 2\sigma\theta$, where σ stands for the right- and left-spinning circularly polarized light, and θ stands for the nanopillar orientation angle. Next, to improve the cross-polarization component, we optimize the geometric parameters of the nanopillar. The horizontally placed nanopillars are dimensionally scanned at an operating wavelength of 532 nm over the range of 60 nm to 240 nm with a scanning step of 2 nm. By using the periodic boundary conditions for the simulations, we obtain the results for the polarization conversion efficiency (PCE), which is defined as the proportion of the cross-polarized component in the transmitted wave, and the corresponding phase difference under the x- and y-polarized incident lights as illustrated in Fig. 3(b), (c).

Based on the simulations of the above section, we set the length and width of the ideal nanopillar as $L = 230$ nm and $W = 74$ nm, respectively, indicated by the white pentagram in Fig. 3(b). At this size, the nearly π phase delay between the long and short axes allows the nanopillar to behave as a half-wave plate, which results in an efficient polarization conversion efficiency. Next, for a fixed-size of nanopillar, we also simulate the normalized cross-polarized component intensity of the nanopillar at circularly polarized incidence with a wavelength from 450 to 650 nm. As illustrated in Fig. 3(d), the selected nanopillar consistently maintains a high cross-polarized intensity over a wide wavelength range, indicating the broadband operation capabilities of the designed metasurface in the visible wavelength range.

B. Design of Metasurface for Generating PEPV Arrays With Uniform Topological Charges

Consider next a designed metasurface for generating 1×5 and 5×5 arrays of PEPV beams. The phase distribution is integrated by the Dammann grating phase and the power-exponent phase. Taking the one-dimensional vortex array as an example and combining it with (2), the transmission function can be written as:

$$T = \exp(i\varphi_{DG}) \cdot \exp(i\varphi_{PEPV}) = \sum_{m=-\infty}^{+\infty} C_m \exp\left(i\frac{2m\pi x}{T_x}\right) \cdot \exp\left[i \cdot 2\pi l\left(\frac{\theta}{2\pi}\right)^{\alpha}\right]. \quad (5)$$

According to the numerical solutions of the optimized phase transition points at different beam splitting ratios given in [19], for the one-dimensional 1×5 Dammann grating, the optimized phase transition points within a cycle are 0.03863, 0.39084, and 0.65552 when the grating has a high conversion efficiency. As illustrated in Fig. 4(b), the one-dimensional Dammann grating phase consists of 12 cycles with only 0 or π phase values. Since the metasurface is a discretized phase modulation device, each cycle of the grating consists of 26 dot positions, and the phase transition points are applied at the 1st, 10th, and 17th dot positions, respectively. As illustrated in Fig. 4(c), the phase distribution used to generate PEPV arrays of the same topological charge is obtained by multiplying the one-dimensional Dammann grating phase with the PEPV phase, where the topological charge and the power order are 6 and 2, respectively. After that, based on the principle of geometrical phase modulation of the metasurface, the phase profile is discretely applied to the angular modulation of the nanopillars within each cell of the metasurface. The cross-polarized channels' far-field diffracted electric field intensity distribution is simulated under a circularly polarized light ($\lambda = 532$ nm). As illustrated in Fig. 5(a), a C-type vortex array with uniform intensity and similar outline size is obtained on the center of the far-field projection which is calculated on a hemispherical surface located 1 m away.

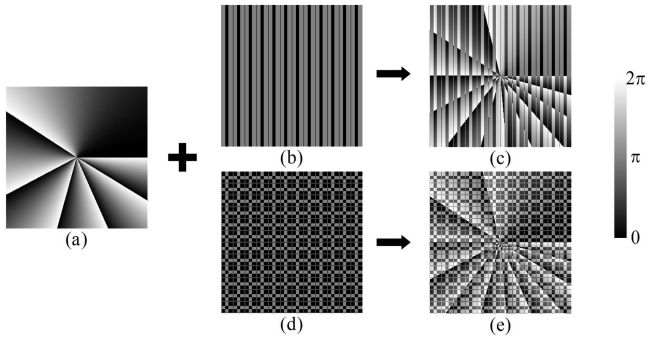

Fig. 4. (a) Phase profile of PEPV with topological charge $l = 6$ and power order $\alpha = 2$; (b) The phase profiles of 1D Dammann grating producing 1×5 spots; (c) The phase profile that results from integrating (a) and (b); (d) The phase profiles of 2D Dammann grating producing 5×5 spots; (e) The phase profile that results from integrating (a) and (d).

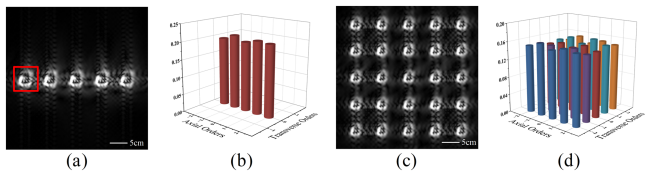

Fig. 5. (a), (c) Far-field diffraction patterns of 1D and 2D PEPV arrays; (b), (d) The intensity distribution of 1D and 2D PEPV arrays in different diffraction orders.

To visually analyze the uniformity of the vortex intensity at each diffraction order, we uniformly divide the vortex array into five square regions according to the diffraction order (the red-boxed region in Fig. 5(a)), and compute the average electric field intensity of each region, which results in the distribution of the intensity at each diffraction order as shown in Fig. 5(b). Further, using the average electric field strength of each diffraction order as the data source, the uniformity of the electric field strength of the one-dimensional vortex beam is calculated to be 0.966 according to the universal uniformity formula $Q = 1 - (I_{\max} -$

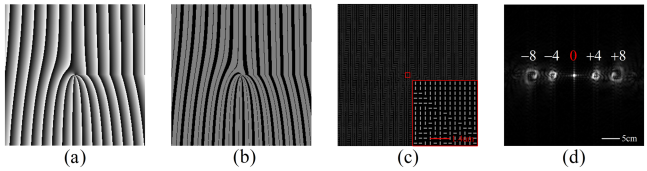

Fig. 6. (a) Phase profile of PEPV grating with $l = 4$, $\alpha = 2$; (b) The phase profile of the PEPDVG with $l = 4$, $\alpha = 2$; (c) Top view of the metasurface and a partial enlarged view of its central area; (d) The simulated intensity distribution of 1D PEPV arrays in different diffraction orders.

$I_{\min})/(I_{\max} + I_{\min})$, where $I_{\max}$ and $I_{\min}$ are the maximum and minimum values of the average electric field strength of all regions.

In addition, similar to the one-dimensional Dammann grating, extension to two dimensions is straightforward. The two-dimensional Dammann grating can generate arrays of equally spaced, uniformly intense light points in the two-dimensional plane. The phase distribution of a 5 × 5 array of PEPV beams with the same topological charge is performed, as illustrated in Fig. 4(d), (e), by combining the PEPV phase with the 2D Dammann grating phase. Then the generated phase profile is encoded by a dielectric geometric metasurface by adjusting the orientation angle of the corresponding nanopillar. The far-field diffraction pattern produced by the simulation, depicted in Fig. 5(c), shows a 5 × 5 array of PEPV beams with equal space, uniform intensity, and similar profile. The diffraction results are further divided into uniform regions and the average electric field intensity is calculated to obtain the intensity distribution of each diffraction order as illustrated in Fig. 5(d). The uniformity of the electric field intensity of this array of beams is calculated to be 0.937.

C. Design of Metasurface for Generating PEPV Arrays With Different Topological Charges

The conventional Dammann vortex grating (DVG) is obtained by phase binarization on the basis of vortex grating. Referring to (3), the Dammann vortex grating is capable of generating multiple optical vortices with equal energy distribution and carrying different topological charges. In this paper, we propose that the phase distribution of the power-exponent-phase Dammann vortex grating (PEPDVG) is obtained by phase binarization on the basis of the PEPV grating. The binarized phase distribution corresponds to only two values of the orientation angle of the nanopillars of the metasurface and thus is also simpler and more feasible in the fabrication of the metasurface. As illustrated in Fig. 6(a), (b), the phase of a PEPV grating is binarized according to the phase transition point of a 1 × 5 Dammann grating to obtain the phase distribution of a 1 × 5 PEPDVG, where the basic topological charge $l = 4$ and the basic power order $\alpha = 2$, respectively.

The far-field diffraction pattern is shown in Fig. 6(d), and a one-dimensional array of PEPV beams with vortex shapes related to the diffraction order is obtained in the far-field plane. It is observed that PEPV beams with the same size and opposite

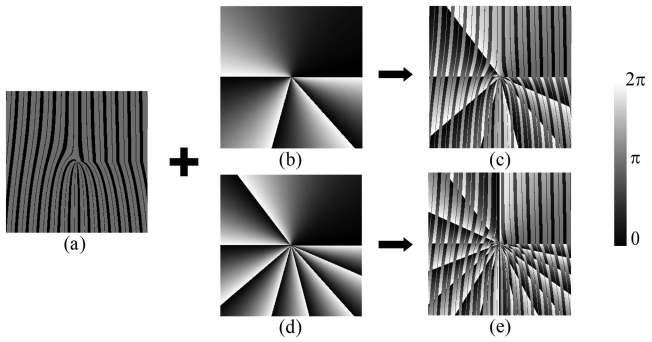

Fig. 7. (a) Phase profile of PEPDVG with $l = 4$, $\alpha = 2$; (b) The phase profiles of the PEPV beam with $l = 4$, $\alpha = 2$; (c) The phase profile that results from integrating (a) and (b); (d) The phase profiles of the PEPV beam with $l = 8$, $\alpha = 2$; (e) The phase profile that results from integrating (a) and (d).

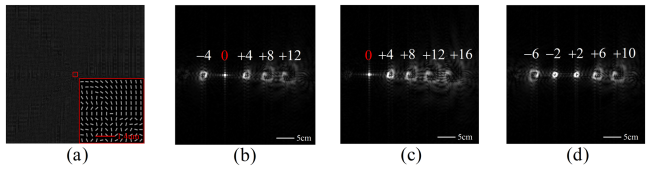

Fig. 8. (a) Top view of the metasurface and a partial enlarged view of its central area; Simulation results of the far-field diffraction patterns of metasurfaces by adding PEPV phases of different topological charges (b) $l = 4$, $\alpha = 2$, (c) $l = 8$, $\alpha = 2$, and (d) $l = 2$, $\alpha = 2$ on PEPDVG with $l = 4$, $\alpha = 2$, respectively.

openings appear at the 1 and −1 diffraction orders, and the vortex profile increases with the absolute value of the diffraction order.

Further, we can add parameter-specific PEPV phases to the PEPDVG to realize the detection of the topological charge of each diffraction order of the grating. As illustrated in Fig. 7, the new phase distributions were obtained by adding PEPV phases with $l = 4$, $\alpha = 2$, and $l = 8$, $\alpha = 2$ to a PEPDVG with $l = 4$, $\alpha = 2$. As shown in Fig. 7(c), (e), theoretically, the topological charges of each diffraction order on the new diffraction pattern are obtained by adding the topological charges of the original PEPDVG with l. The far-field diffraction pattern shows a solid spot at the positions of −1 and −2 orders in Fig. 8(b) and (c), respectively. This indicates that the corresponding vortex's topological charge is zero. It follows that the topological charge of the vortex at this diffraction order in the original PEPDVG diffraction field can be verified by the position of the solid spot. Indeed, this proposed method increases the flexibility of topological charge modulation in PEPV beam arrays. As illustrated in Fig. 8(d), when superimposing a PEPV phase of $l = 2$, $\alpha = 2$, it is possible to obtain PEPV beams with topological charges of $l = -6$ and $l = -2$ at orders −2 and −1, respectively, which is not possible using a single PEPDVG alone.

D. Testing of Variability in Number and Shape of Vortex Arrays and Bandwidth of Grating

According to the Dammann grating principle, the number of arrays can be flexibly changed by changing the optimized phase transition points within a cycle. When the phase transition

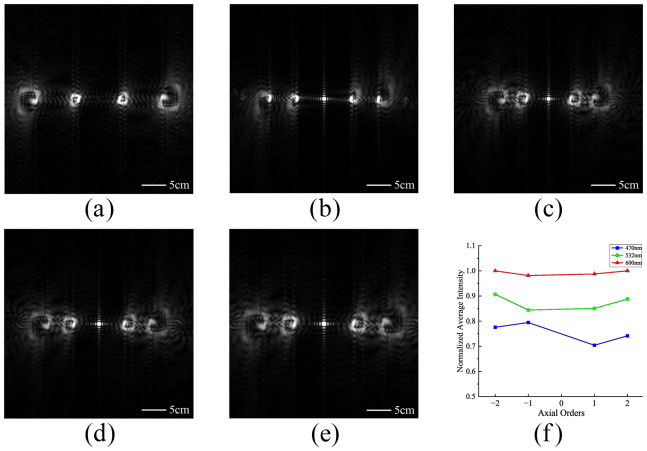

Fig. 9. Simulation results of the far-field diffraction patterns with different factors of the PEPDVGs. (a) $l = 4$, $\alpha = 2$, 1×4, $\lambda = 532$ nm; (b) $l = 6$, $\alpha = 4$, 1×5, $\lambda = 532$ nm; (c) $l = 6$, $\alpha = 2$, 1×5, $\lambda = 470$ nm; (d) $l = 6$, $\alpha = 2$, 1×5, $\lambda = 532$ nm; (e) $l = 6$, $\alpha = 2$, 1×5, $\lambda = 600$ nm; (f) Normalized average intensity of far-field diffraction patterns of PEPDVG with $l = 6$, $\alpha = 2$, 1×5, $\lambda = 470, 532, 600$ nm.

points per unit cycle are 0.22057, 0.44563, 0.5, 0.72057, and 0.94563, a beam splitting of the 4th order can be formed. To realize the proximity of the phase transition points, the number of pixels per unit cycle of the Dammann grating is set to 32. As shown in Fig. 9(a), we designed a PEPDVG metasurface and successfully generated an array of 1×4 PEPV beams in the far-field diffraction pattern.

As a comparison, we make changes to the topological charge and power order of the underlying PEPV phase and simulate the corresponding far-field diffraction results separately. Comparing Fig. 6(d) with Fig. 9(c), note that at the same diffraction level, the size of the spot increases as the topological charge number of the base PEPV phase increases, but the spiral shape does not change. In addition, increasing the power order results in a more concentrated intensity distribution of the beam, as shown in Fig. 9(b). From the analysis and discussion above, in the base PEPV phase, the profile size, opening direction, and intensity distribution of the spot in the vortex array depend on the magnitude and sign of the topological charge, and the magnitude of the power order.

Finally, the designed metasurfaces are simulated at incident circularly polarized light wavelength of 470 nm and 630 nm, as illustrated in Fig. 9(d), (e). Because of chromatic aberration of magnification, the size of the vortex will expand as the wavelength increases. At visible wavelengths, the high refractive index, low loss of TiO_2 nanopillars and the wavelength-independent properties of PB phase are the keys to the broadband practicality of our proposed metasurface. We calculated the average electric field intensity for each vortex in the vortex array at three discrete wavelengths. As illustrated in Fig. 9(f), the generated PEPV beam arrays maintain high efficiency and uniformity at different wavelengths, which indicates that the designed metasurfaces have the broadband operation capabilities of PEPV beam array generation in the visible wavelength range.

IV. Conclusion

In summary, we propose the use of metasurface optics to realize the generation of PEPV arrays. First, a dielectric metasurface for generating PEPV arrays with identical topological charges and uniform intensities is designed by combining the equally spaced, equally intense beam splitting properties of Dammann gratings with the power-exponent-phase. Secondly, with reference to the theory of conventional Dammann vortex grating, the power-exponent-phase is replaced with the conventional vortex phase to design the dielectric metasurface loaded with the PEPDVG phase. This metasurface is used to generate PEPV arrays with topological charges related to the diffraction order. The proposed metasurface can be flexibly used for PEPV array generation as well as efficient operation at broadband. Therefore, the proposed method can provide a new way for multi-particle capture and transfer, optical communication, etc.

References

[1] P. Coullet, L. Gil, and F. Rocca, "Optical vortices," *Opt. Commun.*, vol. 73, no. 5, pp. 403–408, 1989.
[2] L. Allen, M. W. Beijersbergen, R. Spreeuw, and J. Woerdman, "Orbital angular momentum of light and the transformation of Laguerre-Gaussian laser modes," *Phys. Rev. A*, vol. 45, no. 11, 1992, Art. no. 8185.
[3] G. D. Jeffries, J. S. Edgar, Y. Zhao, J. P. Shelby, C. Fong, and D. T. Chiu, "Using polarization-shaped optical vortex traps for single-cell nanosurgery," *Nano Lett.*, vol. 7, no. 2, pp. 415–420, 2007.
[4] M. Padgett and R. Bowman, "Tweezers with a twist," *Nature Photon.*, vol. 5, no. 6, pp. 343–348, 2011.
[5] D. Gao et al., "Optical manipulation from the microscale to the nanoscale: Fundamentals, advances and prospects," *Light: Sci. Appl.*, vol. 6, no. 9, pp. e17039–e17039, 2017.
[6] J. Wang et al., "Terabit free-space data transmission employing orbital angular momentum multiplexing," *Nature Photon.*, vol. 6, no. 7, pp. 488–496, 2012.
[7] N. Bozinovic et al., "Terabit-scale orbital angular momentum mode division multiplexing in fibers," *Science*, vol. 340, no. 6140, pp. 1545–1548, 2013.
[8] Y. Ren et al., "Orbital angular momentum-based space division multiplexing for high-capacity underwater optical communications," *Sci. Rep.*, vol. 6, no. 1, 2016, Art. no. 33306.
[9] S. Fürhapter, A. Jesacher, S. Bernet, and M. Ritsch-Marte, "Spiral interferometry," *Opt. Lett.*, vol. 30, no. 15, pp. 1953–1955, 2005.
[10] K. I. Willig, S. O. Rizzoli, V. Westphal, R. Jahn, and S. W. Hell, "STED microscopy reveals that synaptotagmin remains clustered after synaptic vesicle exocytosis," *Nature*, vol. 440, no. 7086, pp. 935–939, 2006.
[11] C. A. Alonzo, P. J. Rodrigo, and J. Glückstad, "Helico-conical optical beams: A product of helical and conical phase fronts," *Opt. Exp.*, vol. 13, no. 5, pp. 1749–1760, 2005.
[12] J. B. Götte et al., "Light beams with fractional orbital angular momentum and their vortex structure," *Opt. Exp.*, vol. 16, no. 2, pp. 993–1006, 2008.
[13] H. Li and J. Yin, "Generation of a vectorial Mathieu-like hollow beam with a periodically rotated polarization property," *Opt. Lett.*, vol. 36, no. 10, pp. 1755–1757, 2011.
[14] P. Li, S. Liu, T. Peng, G. Xie, X. Gan, and J. Zhao, "Spiral autofocusing airy beams carrying power-exponent-phase vortices," *Opt. Exp.*, vol. 22, no. 7, pp. 7598–7606, 2014.
[15] G. Lao, Z. Zhang, and D. Zhao, "Propagation of the power-exponent-phase vortex beam in paraxial ABCD system," *Opt. Exp.*, vol. 24, no. 16, pp. 18082–18094, 2016.
[16] W. Luo, S. Cheng, Z. Yuan, and S. Tao, "Power-exponent-phase vortices for manipulating particles," *Acta Opt. Sinica*, vol. 34, pp. 93–97, 2014.
[17] H. Dammann and K. Görtler, "High-efficiency in-line multiple imaging by means of multiple phase holograms," *Opt. Commun.*, vol. 3, no. 5, pp. 312–315, 1971.
[18] G. J. Swanson et al. *Binary Optics Technology: The Theory and Design of Multi-Level Diffractive Optical Elements*, vol. 854. Cambridge, MA, USA: Massachusetts Inst. Technol., Lincoln Lab., 1989.

[19] R. L. Morrison, "Symmetries that simplify the design of spot array phase gratings," *J. Opt. Soc. Amer.*, vol. 9, no. 3, pp. 464–471, 1992.
[20] C. Zhou and L. Liu, "Numerical study of Dammann array illuminators," *Appl. Opt.*, vol. 34, no. 26, pp. 5961–5969, 1995.
[21] N. Yu et al., "Light propagation with phase discontinuities: Generalized laws of reflection and refraction," *Science*, vol. 334, no. 6054, pp. 333–337, 2011.
[22] M. Khorasaninejad, W. T. Chen, R. C. Devlin, J. Oh, A. Y. Zhu, and F. Capasso, "Metalenses at visible wavelengths: Diffraction-limited focusing and subwavelength resolution imaging," *Science*, vol. 352, no. 6290, pp. 1190–1194, 2016.
[23] H. Cao, R. Yuan, C. Xu, Y. Zhang, and W. Hu, "Broadband decoupled spin and orbital angular momentum detection via programming dual-twist reactive mesogens," *Opt. Lett.*, vol. 46, no. 22, pp. 5751–5754, 2021.
[24] R. Yuan et al., "Spin-decoupled transflective spatial light modulations enabled by a piecewise-twisted anisotropic monolayer," *Adv. Sci.*, vol. 9, no. 23, 2022, Art. no. 2202424.
[25] L. Huang et al., "Volumetric generation of optical vortices with metasurfaces," *ACS Photon.*, vol. 4, no. 2, pp. 338–346, 2017.
[26] X. Zhang et al., "Basis function approach for diffractive pattern generation with dammann vortex metasurfaces," *Sci. Adv.*, vol. 8, no. 40, 2022, Art. no. eabp8073.
[27] D. Wen et al., "Broadband multichannel cylindrical vector beam generation by a single metasurface," *Laser Photon. Rev.*, vol. 16, no. 10, 2022, Art. no. 2200206.
[28] X. Zheng, J. Yang, R. Wang, and T. Lan, "Visible light waveband Dammann grating based on all-dielectric metasurface," *Appl. Opt.*, vol. 61, no. 9, pp. 2184–2191, 2022.